ASME Letters in Dynamic Systems and Control
Online journal at:
https://asmedigitalcollection.asme.org/lettersdynsys

Omid Fakharian
Mechanical Engineering Department,
University of Nevada, Reno,
1664 N Virginia Street,
Reno, NV 89557
e-mail: ofakharian@unr.edu

William S. Nagel
Robotics Engineering Department,
Widener University,
Chester, PA 19013
e-mail: wsnagel@widener.edu

Kam K. Leang
Department of Mechanical Engineering
and Robotics Center,
University of Utah,
1495 E. 100 Street,
Salt Lake City, UT 84112
e-mail: kam.k.leang@utah.edu

Matteo Aureli[1]
Mechanical Engineering Department,
University of Nevada, Reno,
1664 N Virginia Street,
Reno, NV 89557
e-mail: maureli@unr.edu

Engineered Ionic Polymer Metal Composites as Extension Sensors: Theory and Experiments

This article investigates analytically and experimentally the mechano-chemo-electrical behavior of ionic polymer–metal composite (IPMC) and engineered IPMC (eIPMC) sensors under extensional loading. To predict the sensing response of eIPMCs, a detailed model is proposed incorporating a composite layer (CL) for the abraded interface between polymer and electrode. We present open-circuit voltage and short-circuit current sensing predictions derived from this model, and we validate them via experiments on anisotropic extensional loading of IPMCs. Experimental results demonstrate that our sensors' electrical outputs align well with theoretical predictions, thereby validating our findings and enhancing our understanding of eIPMC strain sensor behavior.
[DOI: 10.1115/1.4069646]

Keywords: modeling, sensors and sensor networks, smart structures

1 Introduction

Ionic polymer–metal composites (IPMCs) are a class of polymer-based smart electroactive materials that have recently been the subject of intense research, in view of possible applications in various fields, including bioengineering, soft robotics, human–machine interfaces, and rehabilitation devices [1,2]. IPMCs are valued for their multiphysics properties and their dual functionality as sensors and actuators [3–7]. Most previous research has concentrated on the actuator mode of IPMCs, while less attention has so far been given to their sensing mode. The generally accepted mechanism for sensing in IPMCs lies in the redistribution of electric charges within the electroactive polymer caused by a mechanical stimulus. Within the sensing literature, the primary focus has been on bending mode sensing [8], while a few studies have explored compression sensing [9]. However, due to the low sensitivity of IPMCs in compression, practical applications have been limited. It is generally understood that the low sensitivity of IPMC sensors under compression is primarily due to the microstructural symmetry between their top and bottom interfaces. This symmetry restricts the development of inhomogeneous internal strain during compressive loading, which is essential for effective sensing. Our previous works [10–12] have addressed the low sensitivity issue by introducing the so-called engineered IPMC (eIPMC) materials with superior sensitivity in the compression sensing mode. The novel eIPMCs also exhibit better performance compared to traditional IPMC sensors under bending conditions. The enhanced eIPMC sensitivity in both compression and bending modes inspires us to investigate other loading conditions and sensing modes.

In this work, we study mechano-chemo-electrical transduction of IPMCs and eIPMCs under extensional loading conditions by enhancing our previous approach in Ref. [13]. Transduction in this mode is theoretically expected, as the engineered interfaces will promote inhomogeneous strain upon extension, contrary to the case of ideal IPMCs with flat interfaces.

In our previous work, the composite layer (CL) was analyzed using two-dimensional micromechanics, as the (homogenized) behavior is isotropic under compression. In the present study, we employ three-dimensional micromechanics to model the anisotropic mechanical behavior of the abraded interface as a composite layer in both the directions parallel and orthogonal to the grooves. Through this analysis, we are able to define a new transduction gain, which allows us to reinterpret the circuit model results presented in Ref. [13] for the present case of extensional strain sensing. To the best of our knowledge, there is no comprehensive study on these sensors under extension. Thus, the contributions of this work are as follows: (i) the first-ever investigation of IPMC and eIPMC sensors under extensional loading conditions, (ii) a new micromechanics-based model for studying the anisotropic mechano-chemo-electrical behavior of these sensors, (iii) a new set of voltage and current performance experiments on the sensor response of IPMCs and eIPMCs, and (iv) an investigation of the dynamic behavior of eIPMC sensors.

[1]Corresponding author.

Paper Presented at the 2025 Modeling, Estimation, and Control Conference (MECC 2025), Pittsburgh, PA, Oct. 5–8, Paper No. MECC2025-25.

Manuscript received July 16, 2025; final manuscript received August 18, 2025; published online September 15, 2025. Assoc. Editor: Loucas Louca.

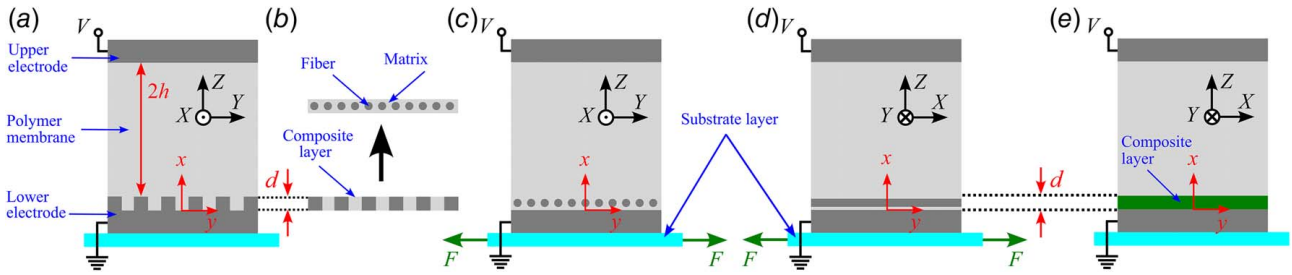

Fig. 1 Schematic representation and nomenclature of the problem: (*a*) eIPMC with one-side abraded polymer. (*b*) Model of the abraded interface to an equivalent fiber–matrix composite lamina. (*c*) eIPMC under extensional loading orthogonal to the groove direction ("orthogonal" eIPMC). (*d*) eIPMC under extensional loading parallel to the groove direction ("parallel" eIPMC). (*e*) Homogenization to mechanically anisotropic composite layer.

2 Problem Statement and Modeling

The problem is schematically depicted in Fig. 1(*a*), along with the relevant nomenclature. We investigate mechano-chemo-electrical transduction through a one-dimensional through-the-thickness (x direction) problem for an eIPMC with semi-thickness h, featuring grounded engineered and free electrodes at $x = 0$ and $x = 2h$, respectively. The eIPMC is fabricated using the polymer abrading technique [11]. During fabrication, one side of the polymer is abraded, and during the plating process, the created grooves are filled with metal. Despite the idealized shape of the grooves in Fig. 1(*a*), the realistic shape of the abrasions was experimentally documented in Ref. [12]. In the absence of more precise information on the microstructure, inaccessible without destroying the sample, we content ourselves with the hypothesis of idealized rectangular grooves and present the qualitative micromechanics results that such hypothesis would imply.

This interface is modeled as a CL comprising a mixture of polymer and metal. This CL is modeled as a unidirectional transversely isotropic fiber-reinforced lamina with metal "fibers" and a polymer "matrix," as shown in Fig. 1(*b*), to capture the anisotropy of the groove microstructure.

To investigate anisotropic sensing, we will consider two different loading conditions in the xy local coordinate system. The extensional load is applied using a substrate at the bottom surface of the sensor, orthogonal, or parallel to the fiber (groove) direction, as depicted in Figs. 1(*c*) and 1(*d*), respectively. These configurations are referred to as "orthogonal" and "parallel" eIPMCs.

The eIPMC sensor model consists of four layers from bottom to top: lower electrode, CL, polymer region, and upper electrode. The CL is modeled as a homogeneous, but anisotropic, layer, as shown in Fig. 1(*e*), so that its mechanical properties differ in the global X and Y directions. To compare the anisotropic functionality of orthogonal and parallel eIPMCs, we also consider a conventional IPMC that does not have engineered interfaces between polymer and electrodes. The conventional IPMC is referred to as the "control" IPMC in the following.

2.1 Micromechanical Model. Previous works on IPMC [9] and eIPMC [13] sensing indicate that inhomogeneous strain in the through the thickness direction is the driver of mechano-chemo-electrical transduction. It is thus essential to understand the mechanical problem of eIPMC strain in the extensional case. To this aim, we formulate a simple micromechanical model to interpret response anisotropy and transduction. We focus on the mechanics of the CL region. The polymer and metal are assumed to be mechanically and electrochemically homogeneous and isotropic. The mechanical properties of the composite layer, based on the micromechanics of a lamina, are expressed using the bridging model of Huang [14]. Accordingly, effective transversely isotropic material properties in the CL depend on polymer and metal elastic constants and volume fractions.

To determine the mechanical behavior of the eIPMC and characterize the dilatation profile driving the sensing behavior, we consider two separate plane strain problems in the xy local coordinate system. These problems involve the quasi-static application of uniform forces F applied to the left and right sides of the substrate layer, see Figs. 1(*c*) and 1(*d*). In both cases, all layers are assumed to be perfectly bonded.

To capture the qualitative dilatation profile in the eIPMC upon application of the forces F, a representative finite element method (FEM) simulation is setup to understand fundamental properties of the strain field. For a given value of the extensional force applied to the substrate, the strain profiles of the eIPMC sample are calculated and shown in Fig. 2. In the representative FEM simulation, a linear and orthotropic behavior is assumed for the composite layer and linear, homogeneous, isotropic elastic behaviors are assumed for both electrodes and polymer layers. Using linear static plane strain FEM analysis, the dilatation fields $\Delta = \varepsilon_x + \varepsilon_y$ were determined based on micromechanical models (as discussed earlier) for both loading conditions applied to the eIPMC, see Fig. 2.

Far from the electrode where the extensional load is applied, the dilatation tends to zero (consistently with free edge condition). Since for enhanced sensitivity it is necessary to exploit the stress concentration generated at the engineered electrode [10], this observation informs the first finding of our study, that is, the eIPMC-engineered electrode must be in the proximity of the applied load in the extensional case. In a practical scenario, the engineered electrode of the stretch sensor eIPMC should therefore

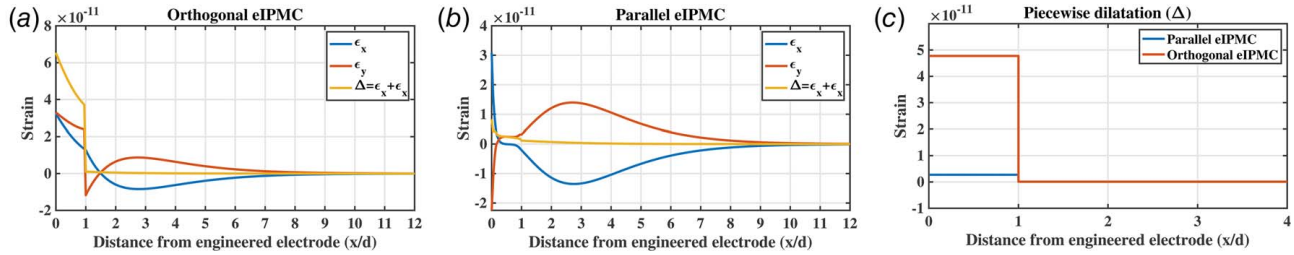

Fig. 2 Finite element results of the strain in the *x* and *y* directions ($\varepsilon_x, \varepsilon_y$), and the dilatation $\Delta = \varepsilon_x + \varepsilon_y$ for (*a*) orthogonal eIPMC and (*b*) parallel eIPMC. (*c*) Piecewise dilatation of the parallel and orthogonal eIPMCs. Mechanical properties of the polymer and metal are $E_m = 171$ GPa, $E_p = 372$ MPa, $G_m = 61.5$ GPa, $G_p = 124.8$ MPa, $\nu_m = 0.39$, $\nu_p = 0.49$, and $V_m = V_p = 0.5$. The composite layer is located in $0 < x/d < 1$, and the polymer region is located in $1 < x/d < 20$.

be attached to the test surface. In this configuration, in the vicinity of the engineered electrode, the strain field is complicated and two dimensional, and the absolute value of the dilatation decreases over the thickness of the composite layer.

The dilatation distribution is required in both CL and polymer regions as an input to the mechano-chemo-electrical analysis. Consistently with the previous minimal mechanical models, we postulate a piecewise constant dilatation field in the eIPMC through the thickness direction. Representative piecewise constant dilatation profiles in the CL and polymer region are shown in Fig. 2(*d*) and are calculated as average values of the dilatation as shown in Figs. 2(*a*) and 2(*b*), between $0 < (x/d) < 1$ and $1 < (x/d) < 20$, respectively. The dilatation fields are written as follows:

$$\Delta_{\mathrm{cl}}(x,\, t) = A_{\mathrm{cl}}\varepsilon_s(t); \quad \Delta_B(x,\, t) = A_B\varepsilon_s(t) \tag{1}$$

where subscripts cl and B indicate the CL and polymer region, respectively, and $\varepsilon_s(t)$ represents the substrate strain caused by the external substrate force F, see Figs. 2(*c*) and 2(*d*). We find that the constant A_{cl} is larger in the orthogonal eIPMC compared to the parallel eIPMC (of a factor of the order of 10). The constant A_B (generally much smaller than A_{cl}) is larger in the parallel eIPMC. The qualitative results of this minimal mechanical model will be used in the next section to couple the electrochemical description of eIPMCs to the external mechanical strain.

2.2 Equivalent Circuit Model and eIPMC Sensor Response. In this section, we develop the equivalent circuit model of the eIPMC sensor and the prediction of open-circuit (OC) voltage and short-circuit (SC) current response. The complete solution process is similar to what described in our previous work [13]. Specifically, while the model and boundary conditions are the same as shown in Ref. [13], the difference lies in the application of extensional strain instead of external compression force. Consequently, the dilatation profile differs, as described by Eq. (1). For completeness, the outline of the solution procedure is provided. Assuming small deformations, electric potentials, and deviations of the counterion concentration from the concentration at rest, we use the generalized linear mechano-chemo-electrical Poisson–Nernst–Planck equations [13] for both the CL and polymer regions. The strain field in Eq. (1) is incorporated as dilation in these equations. After nondimensionalizing the equations and all the boundary, continuity, and initial conditions, the problem is solved analytically using the matched asymptotic expansion method.

After determining the electric potential and counterion concentration fields, the current–voltage relationship of the eIPMC is derived using matching conditions. Thus, the physics-based equivalent circuit of the eIPMC can be determined as shown in Fig. 3. The

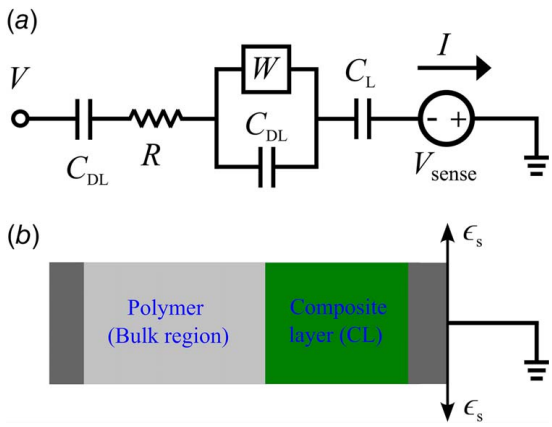

Fig. 3 (*a*) Equivalent circuit of the eIPMC strain sensor. (*b*) Schematic representation of the electrochemical effects under external substrate strain.

dimensional values (per unit nominal eIPMC surface area) of the circuit elements are $C_L = \varepsilon_{\mathrm{cl}}/d$, $C_{\mathrm{DL}} = \varepsilon/\lambda_D$, $W = \varepsilon\sqrt{\mathcal{D}_{\mathrm{cl}}\phi^2/\lambda_D^2}$, and $R = 2h\lambda_D^2/\varepsilon\mathcal{D}$. Here, ε_{cl} and ε are the permittivity of the CL and polymer region, respectively. and $\mathcal{D}_{\mathrm{cl}}$ and $\mathcal{D}$ are the diffusivity of the CL and polymer region, respectively. The parameters d and h are the CL thickness and polymer semi-thickness, respectively. Additionally, λ_D is the Debye screening length, and ϕ indicates the volume fraction of the polymer in the CL. Note, in the circuit, the presence of a Warburg impedance element [15], with impedance $Z_W(s) = 1/(W\sqrt{s})$, which models resistance to mass transfer and is associated with the effect of the CL [16]. Finally, V_{sense} is the sensing voltage, which can be understood as a controlled voltage source, regulated by the external strain.

In the Laplace domain, the dimensional sensing voltage, OC voltage, and SC current are given by

$$V_{\mathrm{OC}}(s) = -V_{\mathrm{sense}}(s) = -\frac{(\mathcal{RT}/\mathcal{F})m\gamma\varepsilon_s(s)}{m+\sqrt{s}} \tag{2}$$

$$I_{\mathrm{SC}}(s) = \frac{(\varepsilon\mathcal{RTD})/(\mathcal{F}h\lambda_D^2)\left(m\sqrt{s}\right)\gamma\varepsilon_s(s)}{2s + (2m)\sqrt{s} + (n+2) + (n+1)m/\sqrt{s}} \tag{3}$$

where s is the Laplace variable, $\mathcal{R}$ is the universal gas constant, $\mathcal{T}$ denotes the IPMC temperature, and $\mathcal{F}$ represents Faraday's constant. In addition, we have defined the nondimensional parameters $\gamma = a_1 - a_2$, $m = \sqrt{\mathcal{D}_{\mathrm{cl}}\phi^2/(\delta\mathcal{D})}$, and $n = d\varepsilon/(h\delta\varepsilon_{\mathrm{cl}})$, with $\delta = \lambda_D/h$.

The parameter m is a measure of the relative diffusivity between the CL and the polymer region, while the parameter n is a measure of relative permittivity between the polymer and CL. Additionally, in Eqs. (2) and (3), the parameter γ is the transduction gain, which depends on the difference in dilatation between the CL and polymer region. This is conceptually similar to the case of a compression eIPMC sensor [10], where γ is a function of the microstructure at the eIPMC polymer–metal interface. However, for the case discussed in this article, γ is also a function of the characteristics of the applied load, as the strain is inhomogeneous even for a conventional IPMC.

2.3 Modeling Results and Predictions. Based on the derived equivalent circuit model of Fig. 3, the model includes three capacitances, function of the permittivity of the bulk polymer and CL, the thickness of the CL, and the Debye screening length. The capacitance C_{DL} in the parallel branch is a double-layer capacitance, developing over a characteristic thickness λ_D, in the vicinity of the CL–electrode interface. The capacitance C_L represents the capacitance associated to the charge storage in the CL, developing over a thickness d. The capacitance C_{DL} represents the double-layer capacitance near the interface between the polymer and the nominally flat electrode. Additionally, R is the through the thickness resistance in the eIPMC due to resistance of the polymer membrane to counterion diffusion. Finally, the Warburg impedance W depends on counterion diffusion within the CL, the permittivity of the bulk region, and λ_D.

Our model assumes that the eIPMC sample has one abraded interface and one nominally flat interface. Although the model is not directly applicable to the control sample with two flat interfaces, we recognize that the actual control sample has some roughness at its polymer–metal interfaces, functioning as thinner CLs [16]. Therefore, we can use the modeling framework to establish a qualitative comparison between the control and eIPMC samples. Based on findings in Ref. [16], $\varepsilon \ll \varepsilon_{\mathrm{cl}}$ and $\mathcal{D} \gg \mathcal{D}_{\mathrm{cl}}$; therefore, IPMCs are expected to have a smaller value for m and a larger value for n compared to eIPMCs. On the basis of these observations, we summarize below the main theoretical predictions of our model, to be verified later with experiments.

(P1) The OC voltage and SC current have a direct correlation with the transduction gain γ. When all other parameters are the same, as $\gamma = a_1 - a_2$ is larger in the orthogonal sample, the orthogonal eIPMC sample exhibits higher OC

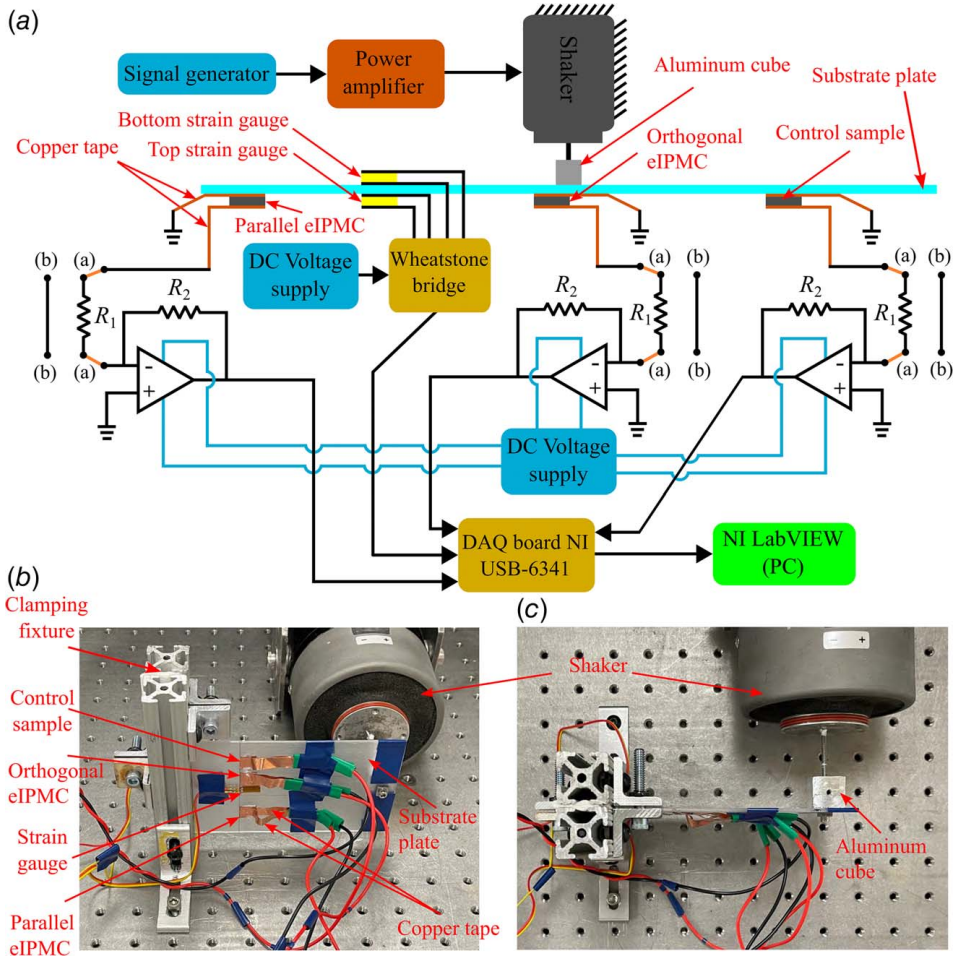

Fig. 4 Experimental setup for eIPMC OC voltage and SC current measurements under extensional strain: (*a*) schematic view, (*b*) isometric view of the actual test setup, and (c) top view of the actual test setup. Connections (a)–(a) and (b)–(b) are used for OC voltage and SC current measurement, respectively.

voltage and SC current sensitivity compared to the parallel eIPMC.

(P2) For moderately low-frequency ranges, the eIPMC OC voltage response tracks the applied external strain. Conversely, the SC current response has high-pass differentiator characteristics, responding to the strain rate.

(P3) For equal applied external strain, the electromechanical properties of the control sample are worse (smaller m and larger n parameters) than the eIPMC sample. From Eqs. (2) and (3), the sensitivity is thus higher for eIPMCs.

3 Experiments

3.1 Experimental Setup. IPMC and eIPMC samples were fabricated as detailed in our previous studies [11,13]. For eIPMC samples, the ionomeric polymer Nafion-1110 is abraded in one direction on a single surface using 220-grit sandpaper to form parallel grooves before standard electroless chemical reduction fabrication. The experimental setup for eIPMC OC voltage and SC current measurements under extensional strain is shown in Fig. 4.

To measure the response to extensional strain on eIPMC and IPMC samples, one surface of the sensors is affixed to a clamped plastic substrate plate undergoing slight bending deformation. Bending deformation is imposed on the plate with a mechanical shaker, see Fig. 4(*c*). A resistive strain gauge, mounted on the plate, serves as reference to measure the actual strain. To ensure pure bending, the imposed displacement is applied precisely at the center of the substrate plate free edge, avoiding torsional displacement in the substrate via the use of an aluminum block. All samples and the reference strain gauge are attached parallel to the clamping fixture, positioned far enough from the plate edges to further ensure equal external strain application to all samples, see Fig. 4(*b*). This setup allows us to apply time varying external strains with different frequencies simultaneously to all samples and the reference strain gauge.

The setup uses a signal generator and a power amplifier to drive the electrodynamic shaker. The shaker stinger is rigidly connected to the plate free edge via the aluminum block, see Fig. 4(*c*). Far from the plate edge, the control sample, orthogonal eIPMC, resistive strain gauge, and parallel eIPMC are attached to the substrate. The eIPMC and IPMC samples, covered with conductive copper tape connected to the data acquisition system, are attached to the substrate plate using liquid cyanoacrylate glue.

Three identical amplification circuits are used for the orthogonal eIPMC, parallel eIPMC, and control IPMC samples, see Fig. 4(*a*). The OC voltage and SC current amplification circuits (inverting amplifier circuit) consist of two resistors, $R_1 = 910\,\Omega$ and $R_2 = 17.75\,\text{k}\Omega$. An LM324N operational amplifier, powered by a DC power supply, is used. The amplified voltages are $V_a = (-R_2/R_1)V_{OC}$ and $V_a = (-R_2)I_{SC}$ in case of OC voltage and SC current measurements, respectively. The amplified voltages V_a are acquired by a NI USB-6341 DAQ board.

Two resistive strain gauges, each with a resistance of $120\,\Omega$ and a sensitivity factor of $2.0 \pm 1\%$, are used. The top strain gauge is attached to the top surface of the substrate plate in the same line

as the eIPMC and IPMC samples, while the bottom strain gauge is attached directly opposite on the underside of the substrate plate, see Figs. 4(*a*) and 4(*b*). These two strain gauges are connected to a Wheatstone bridge circuit, powered by a DC voltage supply. The output voltage from the Wheatstone bridge is connected to the DAQ board. The strain can be calculated using the formula $\varepsilon = 2(V_o - V_{oI})/(SV_s)$, where V_o and V_{oI} are the output voltage and initial output voltage (before deformation), respectively, S is the sensitivity factor of the strain gauge, and V_s is the DC supply voltage of the Wheatstone bridge circuit.

A NI LABVIEW VI (configured with 10,000 samples to read at 1 kHz sampling rate) is used to collect data from the orthogonal eIPMC, parallel eIPMC, control IPMC samples, and the resistive strain gauge.

4 Results

4.1 Quasi-Static Open-Circuit Voltage Response. To experimentally characterize the behavior of the eIPMC sensor, we apply a sinusoidal extensional strain with a frequency of 0.5 Hz and an amplitude of 6×10^{-4} strain to simulate quasi static sensing. Figure 5 shows the actual (measured data divided by amplification gain) OC voltage data for this test. Figures 5(*a*)–5(*c*) show the OC voltage of the control IPMC, orthogonal eIPMC, and parallel eIPMC. For all of these measurements, for clarity of presentation, a low pass filter with $f_{CO} = 15$ Hz is applied to the measurements.

In the limit of zero frequency, from Eq. (2), $V_{\mathrm{OC}}(s) = -(\mathcal{RT}/\mathcal{F})\gamma\varepsilon_s(s)$. By neglecting small phase shift in the sensor output at low frequency, we calculate the static gain between applied strain (as measured by the strain gage) and the sensor voltage output via least square fitting. We find approximately 31 mV/strain for the control IPMC, 50 mV/strain for the parallel eIPMC, and 88 mV/strain for the orthogonal eIPMC. This demonstrates that eIPMC sensors have greatly enhanced sensitivity (almost 300%) compared to conventional IPMC sensors, as per prediction *P*3. As predicted by our micromechanical model prediction *P*1, eIPMCs exhibit a marked anisotropic response, with larger sensitivity in the orthogonal sensing mode, similarly to conventional strain gages.

4.2 Dynamic Open-Circuit Voltage Response to Sine Input Strain. To experimentally investigate the dynamic behavior of the strain eIPMC sensor, we apply various sinusoidal external strain profiles with constant frequencies ranging from 5 Hz to 10 Hz to the setup as described earlier. Throughout this work, we focus on the relatively low-frequency behavior of the eIPMC sensor. In particular, we systematically neglect dynamic effects on the mechanics time scale (which is assumed to respond much slower than the chemoelectrical time scale). To compare the OC voltage sensitivities of the control IPMC, orthogonal eIPMC, and parallel eIPMC samples over different frequencies, the OC voltage sensitivities of all samples at each frequency were calculated and plotted in Fig. 6. The measurement window comprises 10 s of excitation and identification is performed over 1-s windows. Figure 6 thus displays average and standard deviations of the sensitivities for each frequency. The results demonstrate that in all frequency ranges, the eIPMC orthogonal eIPMC shows higher sensitivity than the parallel eIPMC and the control IPMC shows the lowest sensitivity. We find sensitivities of approximately 50 mV/strain, 70 mV/strain, and 70 − 160 mV/strain, for the control, parallel, and orthogonal samples, respectively, demonstrating superior dynamic sensitivity for eIPMC sensors. These results are consistent with predictions *P*1 and *P*3. Before each test at each frequency, we added de-ionized water to each sample using a syringe. The observed dip in the sensitivity of the orthogonal eIPMC at 6 Hz may be attributed to variations in dehydration levels or differing rates of water absorption in the sample before the test at this specific frequency. Since no similar dip is observed in the parallel eIPMC or the control IPMC, it is unlikely that the dip results from frequency-dependent electrochemical relaxation or ionic redistribution dynamics, which typically affect all configurations similarly by reducing net charge separation. Despite these effects, the sensitivities are approximately constant over the studied frequency range, consistently with Eq. (2) and prediction *P*2, that is, the OC voltage output correctly captures the strain.

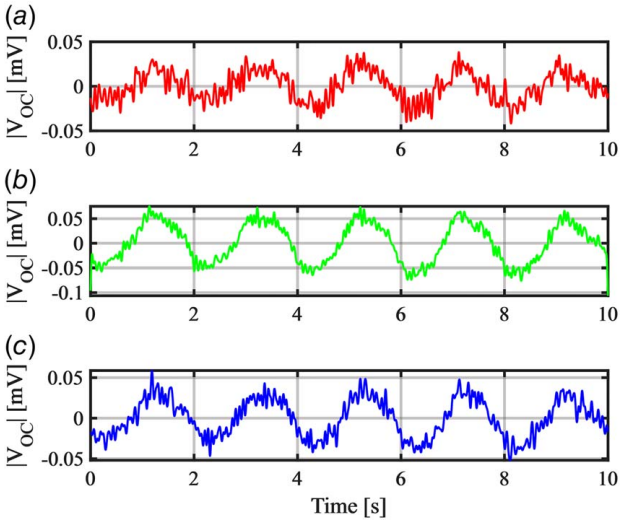

Fig. 5 Actual OC voltage responses to external strain at 0.5 Hz frequency: (*a*) control sample, (*b*) orthogonal eIPMC, and (*c*) parallel eIPMC

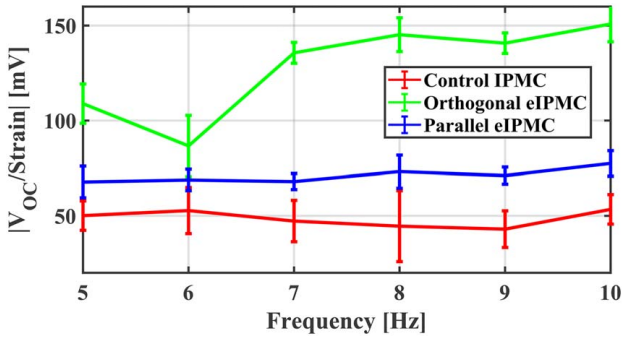

Fig. 6 OC voltage sensitivity for orthogonal, parallel, and control samples. Error bars indicate three standard deviations.

4.3 Dynamic Short-Circuit Current Response to Sine Input Strain. Because of the presence of a $\sqrt{s}$ term in the numerator of Eq. (3), the current response is not sensitive to static strain; therefore, we focus here on the dynamic excitation case. To investigate SC current performance of the strain eIPMC sensor, we apply various sinusoidal extensional strain with constant frequencies ranging from 5 Hz to 10 Hz to the eIPMC strain sensor sample using the setup described earlier.

Similar to the case of OC voltage, SC current sensitivities of all samples at each frequency were calculated. Results are plotted in Fig. 7 along with their error bars. The results show that in all frequency ranges, the orthogonal eIPMC sensor shows higher sensitivity than the parallel eIPMC, and the control IPMC shows the lowest sensitivity. At high frequencies, we find sensitivities of approximately 300 μA/strain, 1100 μA/strain, and 2000 μA/strain, for the control, parallel, and orthogonal samples, respectively, demonstrating superior dynamic sensitivity for eIPMC sensors. These results are consistent with our modeling predictions *P*1 and *P*3.

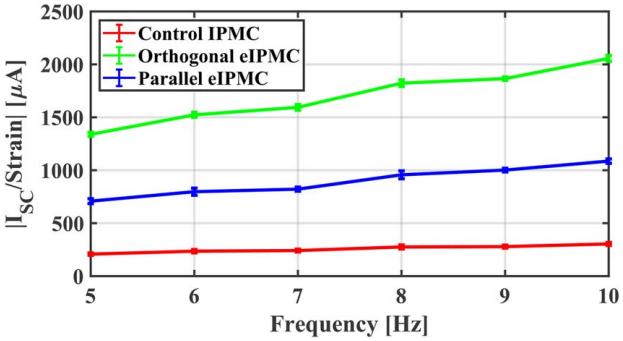

Fig. 7 SC current sensitivities of control and eIPMC samples. Error bars indicate three standard deviations.

The error bars associated with the OC voltage sensitivity were larger than those for the SC current, likely due to the voltage signal's greater sensitivity to electrochemical drift, electrode condition, and environmental noise. In contrast, the SC current reflects more immediate ionic motion and is less affected by long-term or cumulative disturbances, resulting in more consistent measurements. Importantly, consistently with prediction *P*2, the eIPMC sensors in the SC current sensing mode are very suitable for strain rate measurements, as their sensitivity increases as the input frequency increases. A strong linear trend is indeed observed with slopes of approximately 18 μA/strain/Hz, 75 μA/strain/Hz, and 138 μA/strain/Hz, for the control, parallel, and orthogonal samples, respectively.

5 Conclusions

This article investigates, for the first time, the mechano-chemo-electrical behavior of IPMC and eIPMC sensors under extensional strain, both analytically and experimentally. A detailed model incorporating a composite layer for the abraded interface between the polymer and electrode was developed. We presented the OC voltage and SC current sensing predictions derived from this model and validated them via an experimental campaign. Consistent with our previous work, this article focuses on the development of a predictive model of the sensor behavior of eIPMCs based on fundamental physical principles. Necessarily, several simplifying operating assumptions are needed, thus the result in qualitative predictions. In our work, all the qualitative predictions of the model are systematically presented and are experimentally verified, thus supporting our modeling approach and hypotheses.

The experimental results demonstrate superior performance of eIPMC sensors in (quasi)-static and dynamic sensing over conventional IPMCs, whereby voltage measurements are preferable for estimation of strain and current measurements for estimation of the strain rate. In addition, experiments confirm the predicted anisotropic sensing behavior, which is a novel feature of our eIPMC material and is not generally observed in conventional IPMCs. These findings suggest that eIPMC sensors are highly suitable for use under external strain loads, potentially broadening their applications in various soft robotics scenarios. In particular, the anisotropic performance of parallel and orthogonal eIPMC sensors makes them suitable for strain gauge rosette-like configurations, for the determination of the biaxial state of stress at a point, and can thus provide a valuable tool in experimental stress analysis and in feedback control systems.

Acknowledgment

Any opinions, findings, and conclusions or recommendations expressed in this material are those of the authors and do not necessarily reflect the views of the sponsor.

Funding Data

- The National Science Foundation (Grant Nos. 1809852, 1809455, 1847513, and 1545857).

Conflict of Interest

There are no conflicts of interest.

Data Availability Statement

The datasets generated and supporting the findings of this article are obtainable from the corresponding author upon reasonable request.

References

[1] Brufau Penella, J., 2009, "Smart Materials for Microrobotics Motion Control and Power Harvesting," Ph.D. thesis, Universitat De Barcelona, Barcelona, Spain.
[2] Gudarzi, M., Smolinski, P., and Wang, Q.-M., 2019, "Fabrication and Transient Responses of Highly Flexible and Humidity-Insensitive Ionic Polymer–Metal Composites in Different Sensory Modes," J. Intell. Mater. Syst. Struct., **30**(11), pp. 1653–1666.
[3] Hao, Y., Zhang, S., Fang, B., Sun, F., Liu, H., and Li, H., 2022, "A Review of Smart Materials for the Boost of Soft Actuators, Soft Sensors, and Robotics Applications," Chin. J. Mech. Eng., **35**(1), p. 37.
[4] Pérez, P. A. L., Lopez, R. A., and Femat, R., 2020, *Control in Bioprocessing: Modeling, Estimation and the Use of Soft Sensors*, John Wiley & Sons, Hoboken, NJ .
[5] Patel, S., Park, H., Bonato, P., Chan, L., and Rodgers, M., 2012, "A Review of Wearable Sensors and Systems With Application in Rehabilitation. Journal of Neuroengineering and Rehabilitation," J. Neuroeng. Rehabil., **9**(1), p. 21.
[6] Amjadi, M., Kyung, K.-U., Park, I., and Sitti, M., 2016, "Stretchable, Skin-Mountable, and Wearable Strain Sensors and Their Potential Applications: A Review," Adv. Funct. Mater., **26**(11), pp. 1678–1698.
[7] Park, J., Lee, Y., Cho, S., Choe, A., Yeom, J., Ro, Y. G., Kim, J., Kang, D.-H., Lee, S., and Ko, H., 2024, "Soft Sensors and Actuators for Wearable Human–Machine Interfaces," Chem. Rev., **124**(4), pp. 1464–1534.
[8] Porfiri, M., 2019, "Sensing Mechanical Deformation Via Ionic Polymer Metal Composites: a Primer," IEEE Instrum. Meas. Mag., **22**(5), pp. 5–12.
[9] Volpini, V., Bardella, L., Rodella, A., Cha, Y., and Porfiri, M., 2017, "Modelling Compression Sensing in Ionic Polymer Metal Composites," Smart Mater. Struct., **26**(3), p. 035030.
[10] Histed, R., Ngo, J., Hussain, O. A., Lapins, C. K., Fakharian, O., Leang, K. K., Liao, Y., and Aureli, M., 2021, "Ionic Polymer Metal Composite Compression Sensors With 3D-Structured Interfaces," Smart Mater. Struct., **30**(12), p. 125027.
[11] Nagel, W. S., Hussain, O. A., Fakharian, O., Aureli, M., and Leang, K. K., 2022, "Surface Roughness Effects on Ionic Polymer-Metal Composite (IPMC) Sensitivity for Compression Loads," Proceedings of the SPIE Smart Structures and Nondestructive Evaluation. Electroactive Polymer Actuators and Devices (EAPAD) XXIV, Long Beach, CA, Mar. 6–10.
[12] Nagel, W. S., Fakharian, O., Aureli, M., and Leang, K. K., 2023, "Engineered IPMC Sensors: Modeling, Characterization, and Application Towards Wearable Postural-Tactile Measurement," Smart Mater. Struct., **33**(1), p. 015035.
[13] Fakharian, O., Nagel, W. S., Leang, K. K., and Aureli, M., 2025, "Engineered Ionic Polymer Metal Composites (eIPMCs) Under Dynamic Compression Loading Conditions: Theory and Experiments," Smart Mater. Struct., **34**(2), p. 025048.
[14] Shan, M., Zhao, L., and Ye, J., 2022, "A Novel Micromechanics-Model-Based Probabilistic Analysis Method for the Elastic Properties of Unidirectional CFRP Composites," Materials, **15**(15), p. 5090.
[15] Bard, A. J., and Faulkner, L. R., 2001, *Electrochemical Methods: Fundamentals and Applications*, John Wiley and Sons, Inc., Hoboken, NJ.
[16] Cha, Y., Aureli, M., and Porfiri, M., 2012, "A Physics-Based Model of the Electrical Impedance of Ionic Polymer Metal Composites," J. Appl. Phys., **111**(12), pp. 124901.